Scientific Reports

https://doi.org/10.1038/s41598-026-39621-1

Article in Press

Resolving the contradiction between simulation and experimental results of using gold nanoparticles in proton therapy

Received: 6 October 2025

Accepted: 6 February 2026

Published online: 09 February 2026

Cite this article as: Tabbakh F. Resolving the contradiction between simulation and experimental results of using gold nanoparticles in proton therapy. *Sci Rep* (2026). https://doi.org/10.1038/s41598-026-39621-1

Farshid Tabbakh

Resolving the Contradiction Between Simulation and Experimental Results of Using Gold Nanoparticles in Proton Therapy

Farshid Tabbakh

Nuclear Science and Technology Research Institute, Plasma and Nuclear Fusion Research School, Tehran, Iran.
Corresponding author Email:ftabbakh2000@yahoo.com & ftabbakh@aeoi.org.ir

Abstract: While gold nanoparticles (GNP)s in proton therapy are widely assumed to exert radio-sensitization via mechanism of secondary electron emission, the discrepancies between simulations and experimental outcomes shows that, in some cases, the secondary electron hypothesis fails to explain the experimental observations particularly distant DNA damage beyond the range of low-energy electrons. These persistent discrepancies show weaknesses of this mechanism, as noted by multiple studies. Resolving the long-standing discrepancy is the main purpose of present research. We predict the survival fractions and sensitization enhancement by Geant4 to bridge the gap between simulation and in-vitro data.

Through Geant4 Monte Carlo simulations we demonstrate that proton stopping – not electron emission- by GNPs is the dominant mechanism, driving the GNP enhanced proton therapy via amplification of proton's linear energy transfer (LET).

For the first time, our model successfully reconciles simulation with experimental data by quantifying the key radiobiological parameters: dose enhancement ratio (DER) and sensitization enhancement ratio (SER). These findings redefine GNPs as proton energy modulators rather than electron emitters, resolving the long-standing simulation-experiment discrepancies. However, it is emphasized that, the secondary electron emission from metallic NPs in the range of nano-scale have remarkable impact.

Furthermore, we derive a mathematical relationship between DER and cell survival fraction (SF) in the linear-quadratic (LQ) model with predicted survival curves showing strong agreement with *in-vitro* data.

Keywords: Proton therapy, gold nanoparticles, dose enhancement ratio, sensitization enhancement ratio, cell survival fraction, Geant4

Introduction

Gold nanoparticles (GNPs) are widely employed as radio-sensitizers in radiotherapy, their enhancement mechanisms differ fundamentally between photon and proton therapies. In photon therapy (X- or γ-ray), GNP-mediated effects primarily occur through secondary electron production via Compton scattering, ionization and photoelectric effects [1-4]. However, for proton therapy, an additional mechanism dominates in biological effectiveness enhancement, proton energy loss through coulomb interactions with High-Z materials [5]. For decades, the hypothesis that secondary electrons drive GNP enhancement in proton therapy [6–39] has created a persistent paradox in the field. While Monte Carlo simulations relying on electron-mediated effects predict either negligible dose enhancement [6, 7, 9-13] or only nanometer-scale impacts [14-26], experimental studies consistently report significant increase in cell killing [8, 15, 27-39]. This discrepancy has been repeatedly acknowledged [10, 11, 15, 22, 32, 39]; Peukert et al [22] highlighted that, there is a contradict between simulation and the enhanced dose observed experimentally in both *in-vivo* and *in-vitro*. Sotiropoulos et al [10] also has concluded that, emerging data, challenge the hypothesis of secondary electrons as the radio-sensitizer and thus, the alternative mechanisms must be involved. Moreover, Hespeels et al [32] and Cho et al [15], have emphasized that, the origin of dose enhancement for proton therapy by GNPs is not well understood and additional mechanistic insights are required to explain the experimental observations.

We resolve this fundamental discrepancy by demonstrating that, according to relationship between kinetic energy and linear energy transfer (LET), when protons traversing GNPs, lose their energies to multiple collisions with gold atoms leading to amplification of their LET. The amplified LET (even slightly) will improve the proton's biological effectiveness. Using Geant4 Monte Carlo simulations [40, 41], we show that at clinically relevant concentrations, increasing the proton's LET leads to a significant dose enhancement ratio (DER) matching experimental data. Building on our prior works on the effect of GNPs on proton's LET elevation [42, 43], this study systematically predicts the clonogenic assays in GNP-enhanced proton therapy by modeling of some previous experiments to justify the mechanism ruling the GNP-enhanced proton therapy. In this regard, the empirical data reported by Lin [8], Polf [35], Brero [37], Enferadi [55], Abdul Rashid [56], Cunninghsm [31] have been considered. The agreement with experiments achieved in this study, validates that, the *missing link* in GNP-enhanced proton therapy is proton energy loss to GNPs and completely differs from the mechanism mediate in GNP-photon therapy, the secondary electrons.

Beyond resolving the paradox in proton-GNP enhanced effectiveness, our work provides a mathematical relationship between (DER) and the cell survival fraction (SF) in linear-quadratic (LQ)

model to predict the survival curves of GNP enhanced proton treatment which has been compared with experimental reports.

While, cytoplasmic irradiation primarily generates repairable indirect damage via reactive oxygen species (ROS) e.g., $OH^{\bullet}$ and H_2O_2, the deposited dose in nucleus directly contribute to DNA lesions and cell death [44-49] and hence, in this study, to rigorously evaluate the impact of GNPs on cell response, we have focused on the dose deposited in cell's nucleus [3, 4, 10, 27].

Materials and Methods

The proton's dose in cell nuclei in presence and absence of GNPs was calculated using Geant4 MC tool and then, these parameters have been quantified; dose enhancement ratio (DER), sensitization enhancement factor (SEF), and relative biological effectiveness (RBE) enhancement.

Fig. 1a illustrates the schematic of geometry of the cellular structure (with GNPs included) to clarify the model used in our simulation as has been shown in Fig 1b. In these figures, a volume as a segment within spread-out Bragg peak (SOBP) with the length of 1.24 mm (corresponding to the stopping range of 10 MeV protons) and the spherical cell located at the end of this segment as target. The spherical cell has diameter of 10 μm and nucleus with 5 μm diameter at center [4, 13]. It is emphasized that, the spherical cell models are widely used in simulations [1,4,8,13, 14, 18, 23]. In present simulations, the focus was on the dose deposited in nucleus to study the direct effects while, the GNPs have only concentrated in cytoplasm [1,4,12, 19]. According to Lin et al. [6], when cells take up GNPs, most of the GNPs are internalized through endocytosis and remain in lysosome without access to the nucleus. On the other hand, Chen [3], Liu [4], Li [30] and Carbone [50] reported that, GNPs with size of 2–6 nm were found within both the nucleus and the cytoplasm, while larger GNPs were only located in the cytoplasm. Therefore, the assumption of cytoplasmic concentration of NPs was based on the greater number of publications. The presence of NPs in cell's nucleus also should be considered in some simulations related to ultra-small NPs as well as DER assessment and the electron's contribution ejected from those NPs located in cell's nucleus.

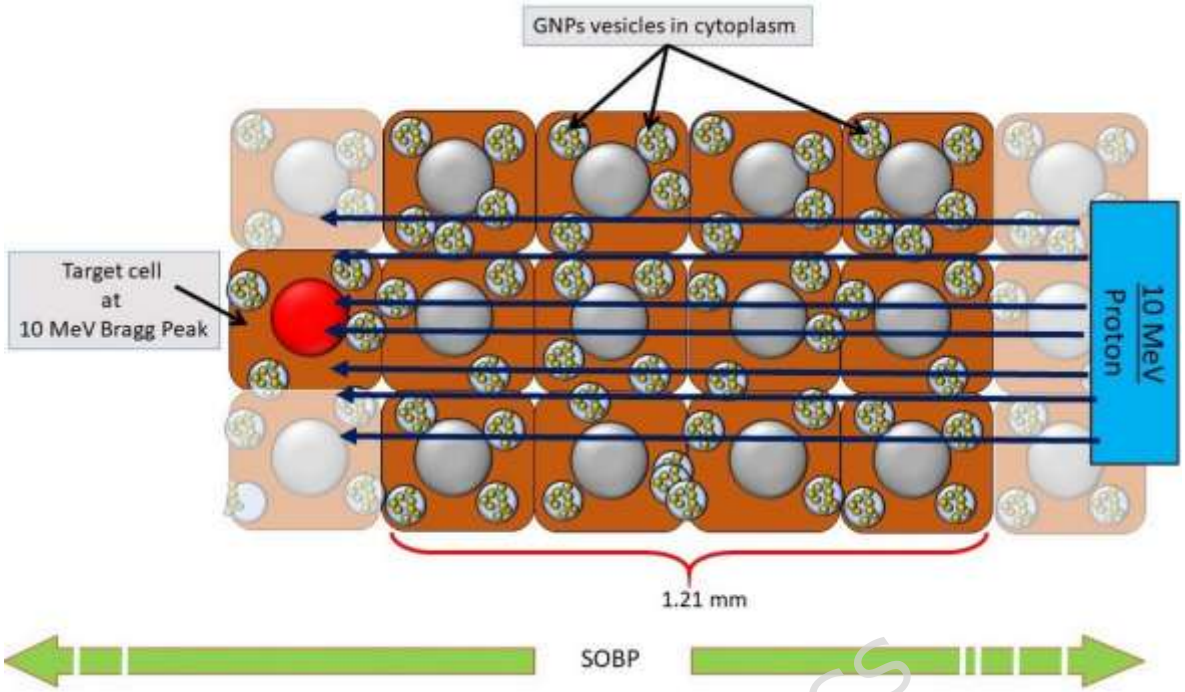

a)

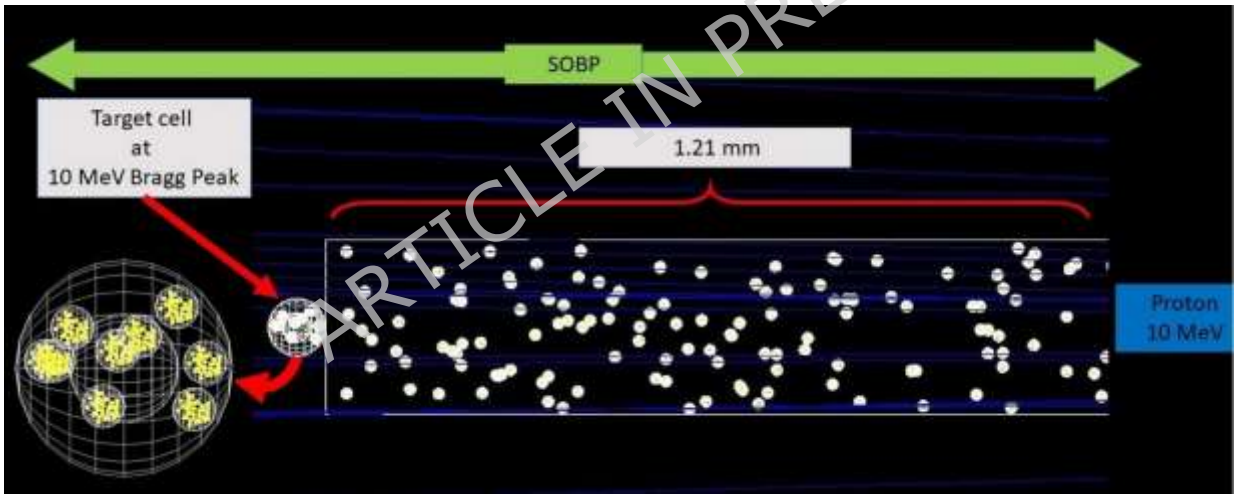

b)

Fig. 1, a) Schematic of intercellular structure of cancerous cells within SOBP and the target cell at the end of range of 10 MeV protons. b) geant4 geometry showing the cell target located at depth of 1.21 mm corresponding to 10 MeV proton's range. The GNP vesicles have been shown

GNP size and Concentration

Different NP's sizes and concentrations were used matching the in-vitro experiments have been presented in Table 1. In our simulations, the GNPs were accumulated in cytoplasm [1, 4, 12, 19] in

vesicles with 200 nm diameter according to Francis [19] and Kwon [51]. The number of GNPs per vesicles was 25 similar to data reported by Rudek [11], Engel et al [1], Liu [4] and also, close to Kwon [51]; 29 GNPs, Pecky [52]; 57 GNPs and Heinfeld [53]; 26 GNPs. However, in modeling based on Enferadi [54] and Abdul Rashid [55] data, almost 5000 ultra-small GNPs were grouped per vesicles to prevent from simulating a huge number of vesicles.

Table 1, NP's materials, sizes and concentrations used in present simulations according to reported in-vitro studies.

Reference	NP material	Size	NP concentration
Lin [8]	GNP	50 nm	$0.2\ \frac{mg}{g}$
Polf [35]	GNP	44 nm	$0.5\ \frac{mg}{g}$
Brero [37]	FeNP	19 nm	$50\ \frac{\mu g}{g}$
Enferadi [54]	GNP	1.8 nm	$45\ \frac{\mu g}{ml}$
Abdul Rashid [55]	GNP - PtNP	1.9 nm - 42 nm	$1\ \frac{mMol}{L}$
Cunninghsm [31]	GNP	50 nm	$10\ \frac{\mu g}{ml}$

Dose Calculation

Dose values were calculated as the deposited energy per mass of target per primary proton;

	$Dose\ (\frac{Gy}{proton}) = \frac{deposited\ energy\ (joules/p)}{mass\ (kg)}$	Equation 1

Dose enhancement ratio (DER) is defined as ratio of the enhanced dose due to presence of GNPs to the dose obtained without GNPs (control dose) [17];

	$DER = \frac{Dose\ (with\ GNPs)}{Dose\ without\ GNPs\ (control)}$	Equation 2

Sensitization enhancement ratio (SER) represents the radiation effectiveness enhanced by GNPs and defined as ratio of the control dose to the GNPs enhanced dose corresponding to the same cell survival fraction (SF) [29, 34];

	$SER = \frac{Dose\ (control)\ with\ SF(10\%)}{Dose\ (with\ GNPs)\ with\ SF(10\%)}$	Equation 3

The DERs related to the mentioned experiments have been quantified first and then, the corresponding survival curve and SERs predicted and compared with the reports.

Survival Fraction (SF) Calculation

Here, we address a predictive method for cell response in GNP combined proton therapy through modification of linear-quadratic (LQ) model parameters, α and β without GNPs in $SF = e^{-\alpha D-\beta D^2}$. This modification was based on mathematical analysis performed by Wenjing et al [56] on relationship between survival fraction and the induced double strand breaks (DSB)s in cell nucleus [56, 57]. Accordingly, the parameters α and β are defined as function of average number of induced DSBs per cell, $N = Y \times D$, in where, Y is average number of induced DSBs per cell per dose (Gy) and D is dose (Gy). It was also assumed that, the distribution of lethal damages in cell nucleus is ruled by Poisson-distribution with average value corresponding to the average number of cell death, $N_{death} \propto N$ [53];

	$-ln\,SF = N_{death} = [-N \times (Parameter1)] \times [1 - N \times (Parameter2)]$	Equation 4

that is [56];

	$SF = e^{-N\times(Parameter1)-N^2\times(Parameter2)}$	Equation 5

Applying $N = Y \times D$ in Equation (5);

	$SF = e^{-(Y\times Parameter1)\times D-(Y^2\times Parameter2)\times D^2}$	Equation 6

then, α and β parameters are;

	$\alpha = Y \times (Parameter1)$	Equation 7

and

	$\beta = Y^2 \times (Parameter2).$	Equation 8

To drive the modified α and β fitting parameters for GNP-enhanced proton therapy, we start from their values without GNP. With considering that, the DSB yield scales linearly with dose, $Yield(DSB) \propto D$ [55, 58-59], we multiply the average number of induced DSBs per cell, $N = Y \times D$ to dose enhancement ratio (DER) to include the linear contribution of enhanced dose hence, $N = Y \times D \times (DER)$ while, $N = Y \times D$ refers to without GNPs treatment (where DER=1).

With applying $N = Y \times D \times (DER)$ to Eq. 5 the modified α and β parameters are;

	$\alpha_{\_modified} = Y \times DER \times Parameter\_1 = \alpha \times DER$	Equation 9

and

	$\beta_{\_modified} = Y^2 \times DER^2 \times Parameter\_2 = \beta \times DER^2$	Equation 10

Finally, the SF values with and without GNPs can be obtained;

	$SF = \begin{cases} e^{-\alpha D - \beta D^2} \rightarrow \ without\ GNPs \\ e^{[-\alpha(DER)]D - [\beta(DER^2)]D^2} \rightarrow \ With\ GNPs \end{cases}$	Equation 11

Our approach, enables prediction of GNP-modified survival curves based on these calculated dose enhancement (DER) and the α and β parameters without GNPs.

Geant4 Setup

Geant4 [40, 41], the general-purpose toolkit for simulating the transport of particles through matter using Monte Carlo techniques was used for present simulations. The version used in this work was Geant4.10.5_p01 in Centos7 Linux operating system. The simulations were conducted according to 10^7 histories per run to minimize the errors to 5 %. The cut-values for proton and electrons were 1 nm [6, 22, 42, 43]. The choice of 1 nm was according other works for better comparison and also because, in the case of secondary electron production, 1 nm gave more confident results. Greater cut-off values give zero electron production according to our simulation.

The hadronic interactions of protons were simulated by *G4HadronElasticPhysicsHP* and *G4HadronPhysicsQGSP_BIC_HP* respectively. The electromagnetic interactions were ruled by G4EmPenelopePhysics as an accurate physics in micro-scale study which tracks the electrons at low energies down to few hundred eV [6, 10]. For more precision, the effect of Auger electrons also was included in simulations by "/process/em/auger true".

Results and Discussion

We calculated the depth dose profile according to protons energy deposition inside the nucleus with and without cytoplasmic GNPs by modeling of Lin [8] Polf [35] and Brero [37] experiments. The results have been depicted in Fig. 2 demonstrating significant enhancement in proton's dose in presence of FeNPs and GNPs. In targeted nucleus, the dose without GNPs, $1 \times 10^{-3}(\frac{Gy}{proton})$ has been increased to $1.25 \times 10^{-3}(\frac{Gy}{proton})$, $1.2 \times 10^{-3}(\frac{Gy}{proton})$ and $1.42 \times 10^{-3}(\frac{Gy}{proton})$ respectively. As one can see in Brero's results, despite the smaller size and concentration of FeNPs, the greater DER is addressed. This is because of larger number of NPs per μm^3 where, in Brero's experiment it was 0.8 $(\frac{NP}{\mu m^3})$ while Lin and Polf have reported 0.2 $(\frac{NP}{\mu m^3})$ and 0.5 $(\frac{NP}{\mu m^3})$ respectively. Due to probabilistic nature of proton interaction with NPs, the number of NPs as well as other quantities of size and weight plays role in dose enhancement as discussed by Penninkx [34] for DER versus gold's weight and size.

Table 2, presents proton's dose with and without gold, Fe and Pt NPs and also, the related DERs obtained from the experiments in Table 1. The dose deposited by secondary electrons also has been included as the evidence of no contribution from electrons in dose enhancement. For better and more clear comparison between proton's DER and of the electrons, data in this table has been visualized in Fig. 3 showing the dose inside nucleus contributed by secondary electrons has not been changed in presence of NPs.

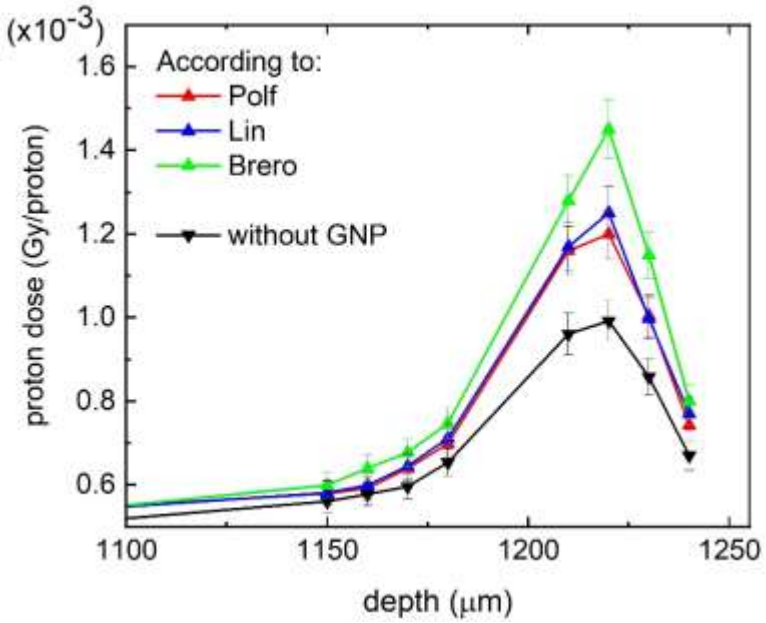

Fig. 2. protons dose deposition along 1200 μm depth of segmented volume with and without GNPs. The elevated curves (green, blue and red) corresponding to NP-enhanced treatment simulation based on Brero [37], Lin [8] and Polf [35] experiments. The black curve represents the dose profile without NPs. These results have error less than 5 %.

Table 2. Dose per proton and DERs related to nucleus at 10 MeV Bragg peak with NPs specifications obtained from the modeling of the reported experiments.

	without NPs ($\frac{Gy}{proton}$)	with NPs ($\frac{Gy}{proton}$)					
		From modeling of Polf [35]	From modeling of Lin [8]	From modeling of Brero [37]	From modeling of Enferadi [54]	From modeling of Cunningham [31]	From modeling of Abdul Rashid [55]
Proton-dose (± 5%) ; (Eq. 1)	1.0×10^{-3}	1.2×10^{-3}	1.25×10^{-3}	1.42×10^{-3}	1.14×10^{-3}	1.22×10^{-3}	1.16×10^{-3} 1.3×10^{-3}
Electron-dose; (± 5%) (Eq. 1)	8.07×10^{-5}	8.08×10^{-5}	8.05×10^{-5}	8.0×10^{-5}	8.01×10^{-5}	8.01×10^{-5}	8.1×10^{-5}
DER (± 5%); (Eq. 2)	-	1.2	1.25	1.42	1.14	1.22	1.16 / 1.3

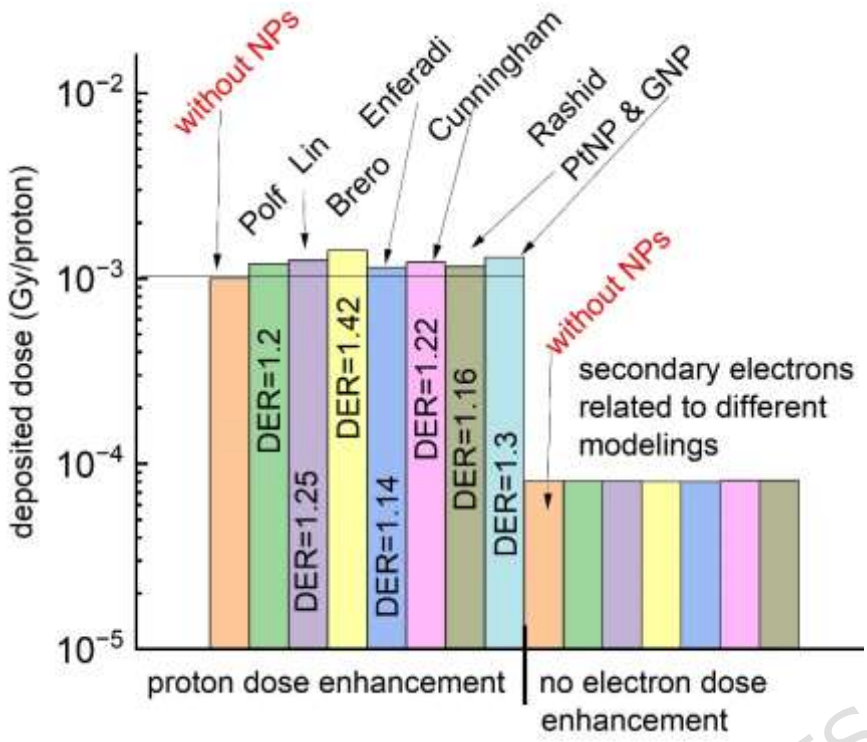

Fig. 3. Data presented in Table 2 has been depicted in this figure for clarifying the significance of proton's dose enhancement ratio (DER) comparing to dose corresponding to the dose contributed by ejected electron from NPs. It is shown no significant increase in electron's dose in presence of NPs.

Evidence for the Mechanism of GNP-enhanced Proton Therapy

Since we have assumed that, there is no GNP in nucleus, one can conclude that, the dose enhancements mostly were only relying on the proton's energy deposition in nucleus. As we saw from Table 2, no dose enhancement by secondary electrons was found in nucleus which is in agreement some researchers claiming that, the electrons ejected from GNPs are not able to contribute to direct DNA damage due to their short range (within nanometer) from GNPs surface [10, 15] leading to doubt on the long-standing hypothesis of secondary electron as the sensitizer in GNP-enhanced proton therapy [10, 11, 15, 22, 32, 39]. The effect of NPs in dose enhancement persists at micrometer scale suggesting that, the protons themselves have caused to enhancement of deposited dose. This has been demonstrated in present work that, the proton's LET has been elevated due to multiple collisions with GNP atoms leading to proton slowed-down and LET elevation consequently. Here, we elucidate the mechanism mediate the GNP-enhanced proton therapy through spectra analysis within nucleus. Fig. 4

compares the energy spectra within the nucleus at Bragg peak for secondary electrons (Fig. 4a) and primary protons (Fig. 4b) with and without GNPs with physical parameters according to Lin [8] and Polf [35]. This figure reveals that, the spectrum of secondary electrons in nucleus remains unchanged (Fig. 4a) indicating that, the secondary electrons emitted from the GNPs do not reach the nucleus over micrometer-scale distances. This also confirm that, the GNP-generated electrons act within cytoplasm and primarily contribute via indirect effects through ROS generation [39].

Fig 4b demonstrate that, the protons spectra significantly increased when GNPs are presented in cytoplasm suggesting a distinct mechanism in effectiveness enhancement. From Fig. 4b, the proton's fluences has been elevated mainly at energies bellow 1 MeV, corresponding to high-LET protons ($>28\ \frac{keV}{\mu m}$). Also, in Table 3, the numerical values of proton's fluences versus energy of protons inside the nucleus are presented for qualitative assessment of elevation of proton's fluence with higher-LET due to metallic NPs. Accordingly, the fluences with GNPs present are significantly greater than without GNPs.

This elevated flux of higher-LET protons provides explanation for the enhanced biological effectiveness observed *in-vitro* with GNPs incorporation. In this context, gold nanoparticles (GNPs) or other High-Z materials enhance the proton electronic stopping power through multiple Coulomb scattering. As protons traverse GNPs, they lose a fraction of their energy via inelastic interactions, resulting in a slightly higher linear energy transfer (LET) upon exiting compared to their initial LET before entering the GNPs. Consequently, as protons propagate along their trajectory, they undergo statistically probable interactions with GNPs, leading to incremental energy deposition and an overall increase in LET before reaching their stopping point. This mechanism has mediated sensitization enhancement in experimental observations. After this elucidation, now we focus on calculating SER verified by reported *in-vitro* experiments.

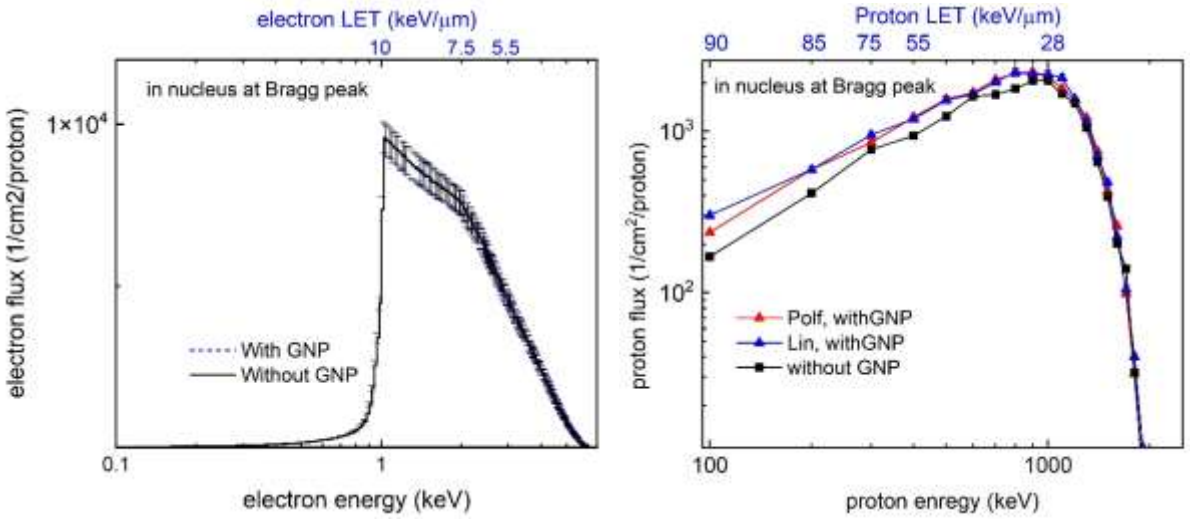

a *b*

Fig. 4. Comparison between energy spectra of *a*) electrons and *b*) protons inside nucleus with and without GNPs assumed to be concentrated in cytoplasm. Left panel shows no significant changes in electron spectra when GNPs are added. In right panel, the spectra of protons without GNPs (black symbols) have been significantly elevated at low energies/ higher-LETs when GNPs added. The blue and red symbols representing the protons spectra according to simulation of the experiments by Lin [8] and Polf [35] respectively. The increase of protons fluence at higher-LET ranges is the evidence of proton stopping by GNPs as the missing mechanism in previous works. (Error bars are included).

Table 3. Tabulated proton's fluence versus energy with and without NPs corresponding to proton's spectra in Fig. 4b, related to modeling the Lin's and Polf's experiments.

Proton's Energy (keV)	Proton's LET ($\frac{keV}{\mu m}$)	Proton's fluence ($\frac{1}{cm^2}$)/proton		
		Without NPs	With GNPs (Lin)	With GNPs (Polf)
100	90	52.3217	75.503	69.688
200	84.3	145.668	210.493	207.311
300	68	304.259	438.97	444.999
400	57	579.011	732.872	789.102
500	50	838.621	1033.26	1057.64
600	43	1104.17	1351.37	1406.46
700	38	1403.07	1766.03	1800.88
800	33.5	1698.11	2122.37	2178.19
900	30	2006.96	2525.33	2560.17
1000	27	2207.28	2895.16	2901.33
1100	26	2374.25	2917.69	2993.45
1200	24	2174.95	2828.69	2876.63
1300	22.4	1973.75	2563.68	2611.61
1400	21	1643.58	2079.07	2101.07
1500	20.4	1129.56	1519.71	1548.84
1600	19.3	752.777	928.268	1000.53
1700	18	409.167	536.802	511.495
1800	17.6	180.767	237.304	247.836
1900	17	78.91	106.87	104.146
2000	16.3	24.4715	30.5216	33.1535
2100	16	7.38502	12.1886	14.1519

Validation of Simulations Using in-vitro Experiments

This study aims to resolve long-standing discrepancy between simulation and *in-vitro* observations in GNP-enhanced proton therapy, which has been puzzling [10, 11, 15, 22, 32, 39]. To achieve this, we predicted GNP treated survival curves according to the simulated DER corresponding to each experiment and Eq. 11 with LQ parameters of without GNP treatment. Using this approach, the DERs corresponding to the experimental conditions reported by Lin [8], Polf *et al* [35] Brero *et al* [37], Enferadi *et al* [54], Abdul Rashid *et al* [55] and Cunningham *et al* [31] were calculated first and then, the SF curves were produced and compared with these reports.

Using the fitting parameters from control curves (without GNPs), we derived the SF curves for GNP-treated conditions. Fig. 5 compares the experimental GNP treated curves (green symbols with solid line) with simulated curves according to DER in Table 2 and Eq. 11 (blue symbols with dashed line). The untreated control curves have been shown according to the reports (black symbols). According to simulated DER=1.25 and control parameters $\alpha = 0.13\ Gy^{-1}$ and $\beta = 0.022\ Gy^{-2}$ from Lin *et al* experiment, Fig. 5a shows that our simulation results for SF curve with GNP is consistent with their data with RMSE almost 1 % Over 8 dose points however, small deviation at doses greater than 7 Gy.

Fig. 5b presents our predicted SF curve based on the obtained DER=1.2 for Polf *et al* experiment. Since α and β values were not provided in their studies, we extracted control parameters manually; $\alpha = 0.49\ Gy^{-1}$ and $\beta = 0.011\ Gy^{-2}$. As shown in this figure, the simulated SF curves demonstrates good agreement with experimental GNP-treated data with RMSE<1 % over 6 dose points.

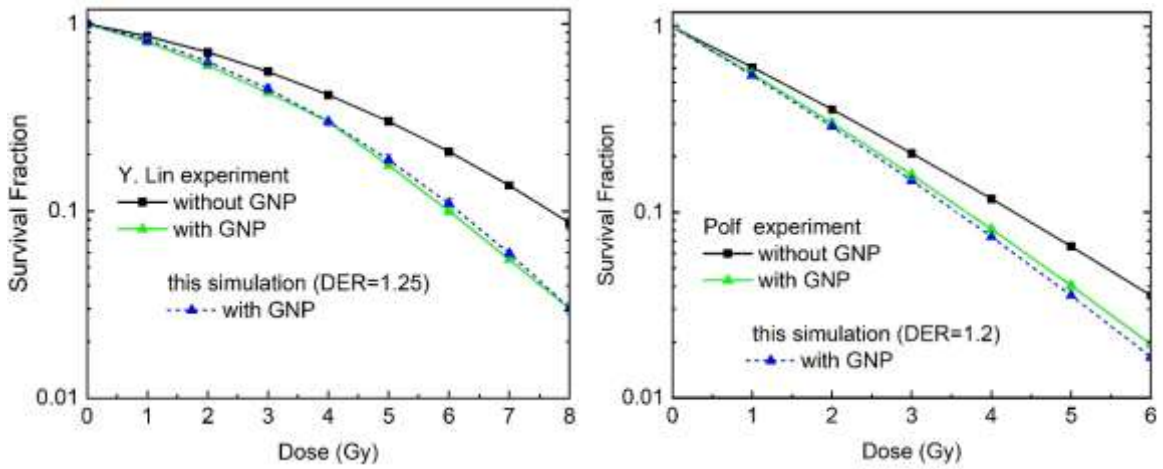

a *b*

Fig. 5. SF curves reported by *a*) Lin and *b*) Polf. For treatment without GNPs (black symbols and solid lines) and with GNPs (green symbols and solid lines). In this figures, the predicted SF curves for GNP treated derived in this study using Eq. 11 and calculated DERs in Table 2 are presented (blue symbols and dashed lines). Both panels show agreement between present simulations and reported experiments. Error bars are included but not visible in logarithmic form.

Further validation was performed by modeling the Brero *et al* [37] and Enferadi [54] proton treatment with iron nanoparticles (FeNP)s and GNPs detailed in Method section. According to original experiment by Brero, dose enhancement at middle of 6 cm SOPB at 12 cm depth was measured after irradiation by proton beam of 131-165 MeV. We simplified the geometry while maintaining physical accuracy using 10-20 MeV protons entering the segmented volume with 1210 μm (Fig. 1). We obtained the proton's spectra in nucleus as depicted Fig. 6a which shows significant elevation in proton's LET in this experiment. Additionally, the tabulated proton's fluence also is presented in Table 4 corresponding to the proton's spectra. For modeling Brero's experiment, the sample were considered at the middle of SOBP region as indicated the origin experiment. Hence, the proton's energy at this point were considered from 10 to 20 MeV to satisfy the realistic condition. The energy steps as presented in Table 4, for Brero's experiment was 500 keV.

According to their report, for without FeNP treatment, $\alpha = 0.63 \pm 0.05\, Gy^{-1}$ and $\beta = 0.015 \pm 0.01\, Gy^{-2}$. Using the calculated DER=1.42 (Table 2) applied into Eq. 11 with mentioned control parameters, the predicted SF curve was derived and compared with their data in Fig. 6. This figure demonstrates good agreement between our model prediction (blue dashed line) and experimental results of FeNP-enhanced proton therapy (green solid line) which also support for the LET elevation mediated by mechanism of protons stopping by High-Z NPs.

Enferadi experiment detailed in Table 1, has been modeled and DER was 1.14. The proton's spectra in target nucleus depicted in Fig. 6c and SF curves corresponding to control and GNP treatment reported by Enferadi compared to this simulation have been shown in Fig. 6d. From Eq. 11 and the obtained DER, the predicted SF curve in this figure (blue dashed curve) shows good agreement with reported GNP treatment (green curve).

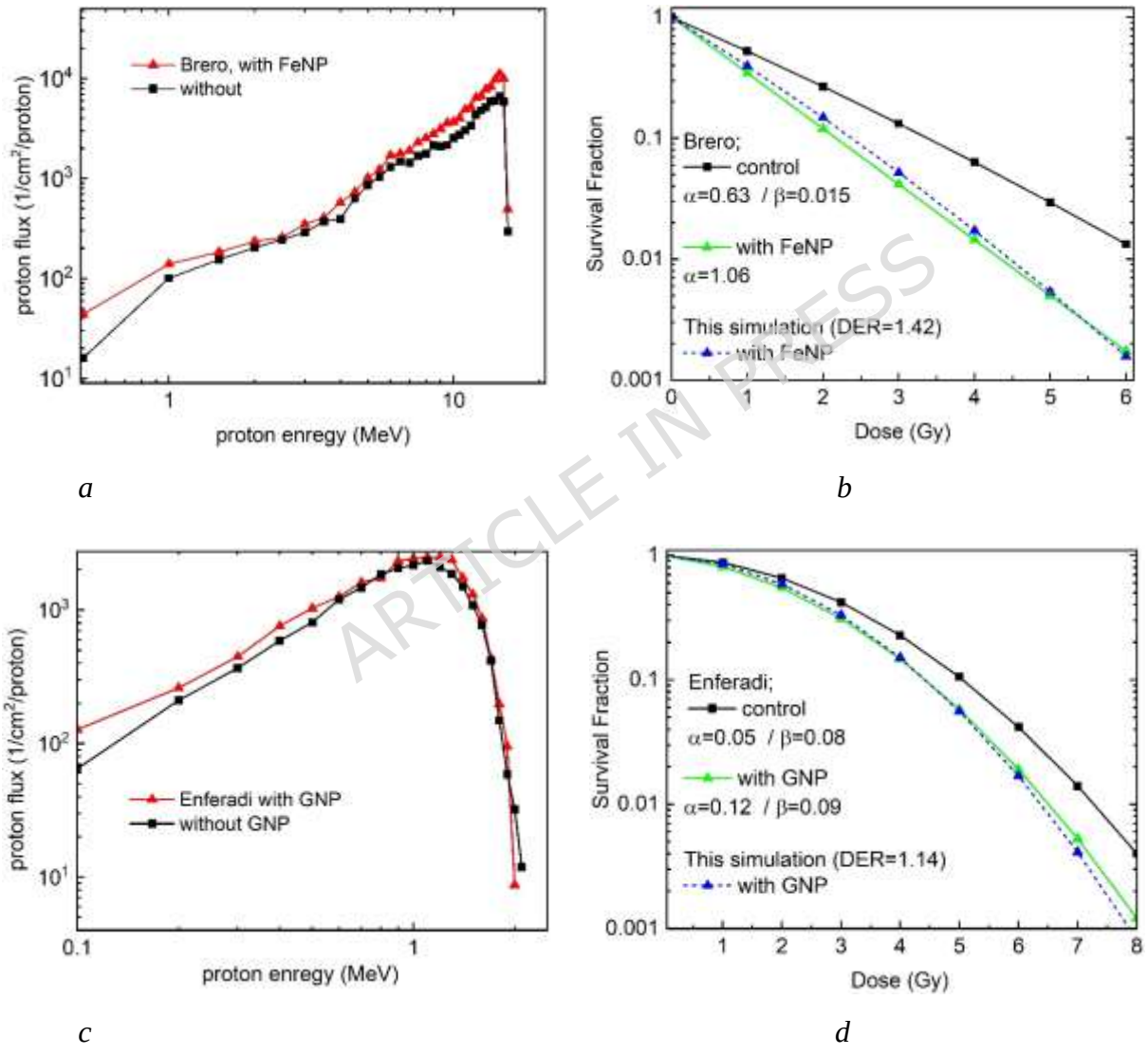

a *b*

c *d*

Fig. 6. another modeling of previous experiment based on Brero's study [37] and Enferadi [54]. *a*) and c) protons spectra with (red symbols) and without (black symbols) NPs. *b*) and *d*) SF curves comparison between reported data (green symbols and solid line) and predicted curve in this study (blue symbol and dashed line). The control curves are also presented (black symbols and solid line). Error bars are included but not visible in logarithmic form.

Table 4. Tabulated proton's fluence versus energy with and without NPs corresponding to proton's spectra in Fig. 6a and 6c, related to modeling the Brero's and Enferadi's experiments.

Proton's Energy (keV)	Proton's LET ($\frac{keV}{\mu m}$)	Proton's fluence ($\frac{1}{cm^2}$)/proton		Proton's Energy (keV)	Proton's LET ($\frac{keV}{\mu m}$)	Proton's fluence ($\frac{1}{cm^2}$)/proton	
		Without GNPs (Brero)	With GNPs (Brero)			Without FeNPs (Enferadi)	With FeNPs (Enferadi)
500	50	16.065	44.1608	100	90	64.8551	127.226
1000	27	100.742	139.65	200	84.3	210.479	260.358
1500	20.5	154.311	182.974	300	68	368.02	447.819
2000	16.3	203.288	235.795	400	57	587.701	758.22
2500	14	244.019	256.712	500	50	808.929	1031.31
3000	12.1	288.31	349.342	600	43	1197.65	1256.43
3500	10.5	369.69	404.46	700	38	1468.44	1609.83
4000	9.5	396.097	573.351	800	33.5	1846.66	1733.77
4500	8.7	633.138	729.261	900	30	2054.86	2330.65
5000	7.96	857.932	1019.17	1000	27	2168.38	2431.98
5500	7.4	1045.45	1230.84	1100	26	2328.04	2480.5
6000	6.9	1295.61	1705.93	1200	24	2092.54	2473.42
6500	6.4	1474.01	1774.54	1300	22.4	1856.54	2376.26
7000	6	1430.99	1902.65	1400	21	1512.18	1745.98
7500	5.7	1686.38	2302.02	1500	20.4	1083.07	1306.2
8000	5.4	1778.62	2541.88	1600	19.3	767.875	859.515
8500	5.2	2141.81	2786.99	1700	18	418.877	432.151
9000	4.97	2107.44	3155.08	1800	17.6	148.76	196.831
9500	4.8	2159.05	3601.74	1900	17	58.8841	95.3555
10000	4.57	2536.64	3687.08	2000	16.3	32.1759	8.72609
10500	4.4	2750.35	4055.67				
11000	4.23	3034.22	4921.25				
11500	4.08	3402.33	5187.4				
12000	3.9	4347.4	6470.54				
12500	3.8	4810.25	6653.2				
13000	3.7	5164.19	7833.87				
13500	3.6	5852.53	8276.66				
14000	3.5	6018.35	9771.27				
14500	3.4	6663.35	11173.2				
15000	3.3	5853.95	10001.9				
15500	3.2	296.039	494.066				

Exceptions and Limitations

During our investigation for assessing the mechanism dominating the GNP-enhanced proton therapy, we found some exceptions when simulating the experiments reported by Abdul Rashid [55] and Cunningham [31] for survival fraction greater than 50 % while there is good agreement between SF curves at 50 % of survival fraction. Also, we have found that, there is limitation for using High-Z nanoparticles in low energy protons as reported by Jeynes [60] experiment using 3 MeV protons.

As it is shown in Fig. 7a-c related to Abdul Rashid, DER was obtained 1.16 and 1.3 corresponding to GNP and PtNP treatment respectively. The SF curves have been produced using these DERs and LQ parameters for control treatment. Figs. 7b and 7*c* show large variation between predicted curves (blue dashed lines) and the reported in-vitro results (green lines). Fig. 7e also, represents the comparison between data reported by Cunningham with the given α and β parameters and predicted curve in present study showing the difference between in-vitro results and simulation despite previous agreements in Figs. 5 and 6. We believed that, uncertainty in modeling or lack of experimental details in geometry could be the reasons for these exceptions. For example, Abdul Rashid has mentioned the PtNPs are in dendrite forms. The position of the sample in phantom, the protons passing the sample with energies greater than 10 MeV are affecting the simulation results. The important point in Cunningham work is the reported LQ parameters which represented in Fig. 7e differs from the figure presented in their published paper [31]. Therefore, the uncertainties in reported LQ parameters also could be the reasons of these exceptions. However, the mechanism of proton slowing-down by NPs and dose enhancement in these exceptions are visible too.

In experiment performed by Jeynes [60] 3 MeV protons irradiated the sample with thickness of only few cells. They have reported no significant increase in sensitization in presence of GNPs. After the modeling, we also have found no elevation in proton's LET because, the length that protons travel within only tens of micrometers are not sufficient to let the protons slowed-down effectively. Sha Li et al [29, 30] have performed another study using ~1 MeV protons and 10 nm and 5 nm GNPs while reporting the significant enhancement in sensitization. These exceptions and limitations which mostly refers to simulation uncertainties are good examples for motivating the researchers to conduct the more accurate simulation and investigate the effect of proton's LET elevation in High-Z NPs combination with proton therapy.

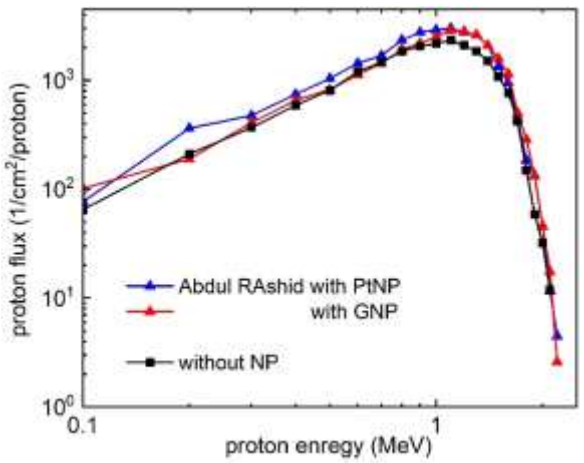

a

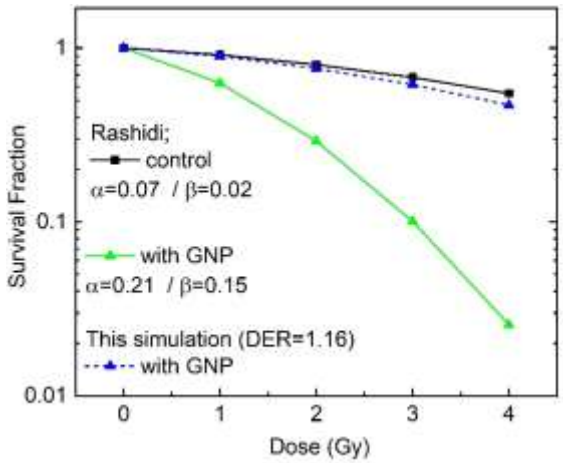

b

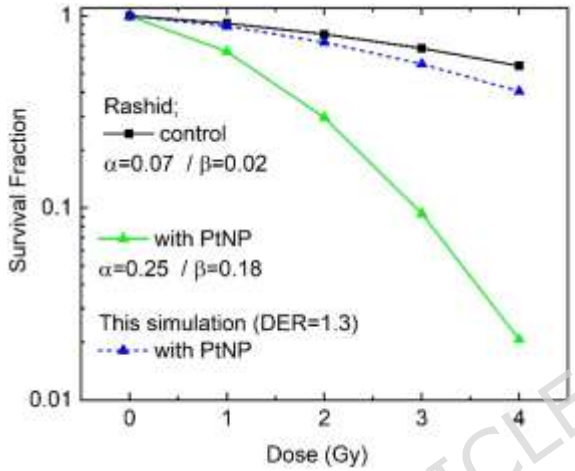

c

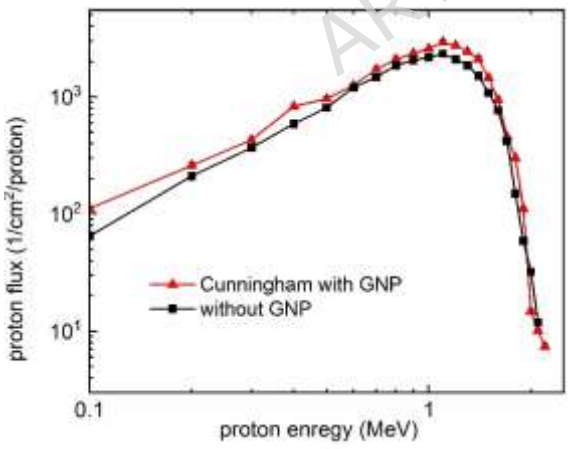

d

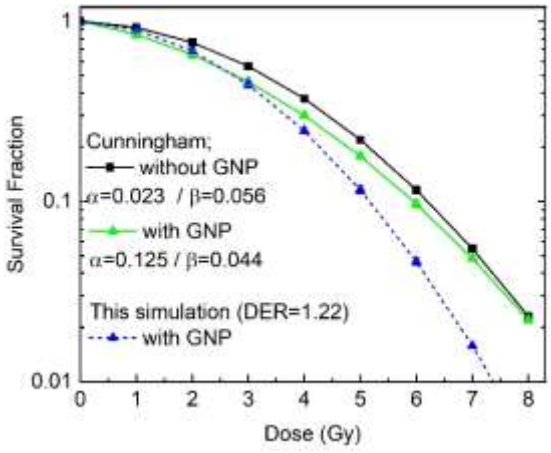

e

Fig. 7. modeling of Abdul Rashid's study [55] a) – c) and Cunningham [31]. d)- e) showing proton's spectra and SF curves. A large variation between simulation (blue dashed curve) and reported data for NP treatment (green curves) were found. The error bars are not visible in logarithmic form.

Table 5. Tabulated proton's fluence versus energy with and without NPs corresponding to proton's spectra in Fig. 7*a* and 7*d*, related to modeling the Rashid's and Cunningham's experiments.

Proton's Energy (keV)	Proton's LET ($\frac{keV}{\mu m}$)	Proton's fluence ($\frac{1}{cm^2}$)/proton			
		Without NPs	With GNPs (Rashid)	With PtNPs (Rashid)	With GNPs (Cunningham)
100	90	64.8551	101.406	76.8126	111.243
200	84.3	210.479	189.161	362.656	259.827
300	68	368.02	407.305	474.567	428.87
400	57	587.701	654.332	744.456	829.733
500	50	808.929	820.413	1038.15	960.285
600	43	1197.65	1122.16	1433.37	1248.36
700	38	1468.44	1433.76	1684.53	1711.06
800	33.5	1846.66	1918.24	2340.97	2083.18
900	30	2054.86	2184.41	2754.8	2350.96
1000	27	2168.38	2496.93	2898.59	2576.85
1100	26	2328.04	2865.53	3017.36	2916.79
1200	24	2092.54	2813.97	2753.13	2739.63
1300	22.4	1856.54	2600.1	2626.62	2438.65
1400	21	1512.18	2089.36	2093	2103.03
1500	20.4	1083.07	1582.76	1327.82	1450.52
1600	19.3	767.875	1143.27	948.294	941.26
1700	18	418.877	500.562	441.386	456.147
1800	17.6	148.76	284.895	184.164	301.026
1900	17	58.8841	131.331	133.947	110.828
2000	16.3	32.1759	45.7278	46.2137	14.6987
2100	16	11.9099	17.4962	11.7294	10.0677

Sensitization Results

As there is a linear relation between Dose and DSB yield, the increase of higher-LET protons (low energy protons) in nucleus due to metallic nanoparticles cause the enhancement of induced dose leading to a greater number of direct damages to DNA including Complex damages and more cancerous cells inactivation in compare to the proton therapy without nanoparticles. In this regard; Folkard *et al* [61] has mentioned that: It is evident from both the proton and the deuteron data that as the energy of the incident particles is reduced (i.e. the average LET increased) the appearance of the survival curves change from low LET in character to high LET. That is, the curves become steeper and shoulder is reduced. Accordingly, when GNPs cause that, the protons lslowed-down their LET increased leading to a sharper Survival Curve which means greater Complex damages and cell death as well.

The sensitization enhancement ratio (SER) for 10 % and 50 % cell survival achieved from both the reported experimental data and present simulation (Figs. 5-7) have been shown in Table 6 as another evidence to verify the agreement between simulations and the reported in-vitro results.

Table6. Sensitization enhancement ratio (SER) for 50 % and 10 % survival achieved by simulation compared with experimental reported data. The errors columns are presented for better justification of the proposed hypothesis.

Experiment by:		SER (50%)			SER (10%)		
		Exp.	Simulation (This work)	error	Exp.	Simulation (This work)	error
Lin [8]		1.34	1.34	0%	1.275	1.3	2.5%
Polf [35]		1.125	1.117	4.5%	1.16	1.21	5%
Brero [37]		1.57	1.47	10%	1.54	1.48	6%
Enferadi [54]		1.16	1.13	3%	1.36	1.36	0%
Cunningham [31]		1.3	1.3	0%	1.08	1.215	13.5%
Abdul Rashis [55]	GNP	2.6	1.18	142%	not provided		
	PtNP	3.1	1.18	~200%			

Discussion

For decades, it was believed that gold nanoparticles (GNPs) in proton therapy functioned via the same mechanism as in photon therapy [1–4], wherein secondary electrons ejected from GNPs drive radiosensitization—same as their role in X-ray or gamma-ray therapy [6–39].

While this hypothesis holds true for photon therapy [1–4], except in nano-scale ranges, it has led to an unresolved paradox in proton therapy.

Simulations indicate no significant increase in direct cell killing [9–13] or only marginal effects mediated by generated ROS [39]—results that starkly contradict in vitro observations. For instance, Rudek et al. [13] reported that electrons below 2 keV fail to reach the nucleus, resulting in a nuclear dose enhancement two orders of magnitude lower than in the cytoplasm. This translates to a mere 0.2% increase in effectiveness, even at GNP concentrations exceeding clinically relevant levels (5% by weight). In contrast, experiments by Polf [35] and Brero [37], using lower nanoparticle concentrations, demonstrated significant increases in direct cell killing and RBE enhancement. This persistent discrepancy between simulations and experimental outcomes has been widely acknowledged [10, 11, 13, 15, 22, 32]." Accordingly, the electron-driven model in proton therapy (unlike in photon therapy) fails to explain DNA lethal damage occurring micrometers away from GNPs accumulated in the cytoplasm. This discrepancy has led some researchers to propose that another mechanism—distinct from secondary electrons—mediates RBE enhancement in GNP-augmented proton therapy. For further clarification:

Sotiropoulos et al [10] have resulted no considerable effect by secondary electrons and hence concluded that, another mechanism could participate in dose enhancement rather than the secondary electrons. From other hand,

Martinez et al [11] has noted that, other effects, such as chemical processes may be responsible for the enhanced radiosensibilization observed in biological studies rather than secondary electrons.

Cho [15] has emphasized that, the origin of GNP effects in proton therapy is unclear.

Peukert et al [22] highlighted that, there is a contradict between simulation and the enhanced dose observed experimentally in both in-vivo and in-vitro.

Hespeels et al [32] have emphasized that, the origin of dose enhancement for proton therapy by GNPs is not well understood and additional mechanistic insights are required to explain the experimental observations.

It is emphasized that, although, impact of the secondary electron generated from ionization of NP’s atoms cannot be ignored specially when the NPs are entered the cell’s nucleus, the alternate mechanisms contributing in SER in proton therapy should be considered too. Hence, the present work aimed to examined the possible mechanism contributing in GNP enhanced proton therapy.

In the present study, by modeling previous experiments (on a smaller scale) and redefining GNPs as proton decelerators rather than electron emitters, we introduce a novel paradigm in precision radiation oncology. This approach bridges the gap between simulations and experimental observations by

elucidating the impact of GNPs on proton linear energy transfer (LET). By the obtained proton's spectra inside nucleus (fluence also are tabulated versus energy), using MC tool, we demonstrated that, the proton's fluence inside nucleus was increased because, the stopping mechanism induced by metallic NPs has forced larger number of proton to be slowed down than without NPs leading to more localized energy deposition and dose enhancement while, without NPs, some of them would pass the nucleus and deposit their energies after the nucleus, somewhere inside the cytoplasm or even in the next cell. In this regard, as the deposited energy can be calculated $\sum_i \ fluence(E_i) \times LET(E_i) \times 1.6 \times 10^{-13}$, by the elevated fluence, the total transferred energy to the place of interest is elevated leading to the total LET elevation and increase of dose [42].

The LET of charged particles depends on the medium's atomic number (Z) [5], following the relationship $\text{LET} = \frac{\text{dE}}{\text{dx}} \propto \text{Z}$. This demonstrates that when protons traverse a medium containing high-Z nanoparticles (e.g., GNPs), they lose more energy per unit distance ($\frac{\text{dE}}{\text{dx}}$), leading to localized LET elevation. As illustrated in Figs. 4*b* and 6*a* (for FeNPs), the presence of High-Z NPs significantly increases the fluence of low-energy protons (< 1 MeV) by several-fold.

This explains the observed dose enhancement (DER > 1) at micrometer-scale distances from NPs—consistent with experimental findings.

By proposing this mechanism as the dominant process in GNP-enhanced proton therapy, we reconcile the longstanding discrepancy between simulations and experiments. Our model accurately predicts survival curves, sensitizer enhancement ratios (SER), and GNP-mediated radiation effects, demonstrating strong agreement with in vitro data.

It is worth to mention that, if the NPs are penetrated in nucleus (for ultra-small NPs), the combination of the two mechanisms of electron production and proton stopping could involving the dose enhancement which needs more justification and verification by the researchers. Also, the chemical reactions between NPs and various cell's enzymes beside the ROS mechanism should be considered as possible mechanisms [62-64].

Conclusion

For the first time**,** this work resolves the long-standing paradox in GNP-enhanced proton therapy by redefining gold nanoparticles as proton energy decelerator rather than electron emitters. Our breakthrough proves that, the GNPs enhance proton therapy primarily through LET elevation (micrometer-scale proton deceleration), directly explaining experimental RBE enhancement, an

outcome the electron-driven model failed to predict. We also, successfully predicted survival curves for GNP/FeNP-enhanced proton therapy with experimental-level accuracy (RMSE <1%). This discovery opens a new era in precision radiation oncology, where nanoscale proton-GNP interactions can be harnessed to maximize clinical efficacy.

References

1. Engels E, et al. Advances in modelling gold nanoparticle radiosensitization using new Geant4-DNA physics models, Phys. Med. Biol., 65, 225017, (2020), DOI: 10.1088/1361-6560/abb7c2.
2. Tudda S. et al, Breast radiotherapy with kilovoltage photons and gold nanoparticles as radiosensitizer: An in vitro study, Med. Phys., 49;568-578, (2022) DOI: 10.1002/mp.15348.
3. Chen Y, Yang J, Fu S and Wu J, Gold nanoparticles as radiosensitizers in cancer radiotherapy, International J of Nanomedicine, 15, 9407-9430 (2020).
4. Liu, R. Zhao T, Zhao X and Reynoson F J, Modeling gold nanoparticle radiosensitization using a clustering algorithm to quantitate DNA double-strand breaks with mixed-physics Monte Carlo simulation. *Med. Phys*. 46(**11**), 5314-5325, (2019) DOI: 10.1002/mp.13813.
5. Carron, N. J., An Introduction to the passage of energetic particles through matter, *1st Edition CRC Press*, Boca Raton. ISBN: 9780429137396, DOI: 10.1201/9781420012378 (2006).
6. Lin Y. *et al*. Comparing gold nano-particle enhanced radiotherapy with protons, megavoltage photons and kilovoltage photons: a Monte Carlo simulation. *Phys. Med. Biol*. **59**, 7675; DOI: 10.1088/0031-9155/59/24/7675 (2014).
7. Lin Y., Paganetti H., McMahon S. J., Schuemann J. Gold nanoparticle induced vasculature damage in radiotherapy: comparing protons, megavoltage photons, and kilovoltage photons. *Med. Phys.* **42**, 5890–5902. DOI: 10.1118/1.4929975 (2015.).
8. Lin Y., McMahon S. J., Paganetti H., Schuemann J. Biological modeling of gold nanoparticle enhanced radiotherapy for proton therapy. *Phys. Med. Biol.* **60**, 4149–4168. DOI: 10.1088/0031-9155/60/10/4149 (2015).
9. Sotiropoulos M. *et al*. Geant4 interaction model comparison for dose deposition from gold nanoparticles under proton irradiation, *Biomedical Physics & Engineering Express*, Volume 3, Number 2, DOI 10.1088/2057-1976/aa69cc (2017).
10. Sotiropoulos M. *et al*. Modelling direct DNA damage for gold nanoparticle enhanced proton therapy, *Nanoscale*, **9**, 18413; DOI: 10.1039/c7nr07310k (2017).
11. Martinez-Rovira I., Prezado Y. Evaluation of the local dose enhancement in the combination of proton therapy and nanoparticles. *Med. Phys*. **42**, 6703–6710; DOI: 10.1118/1.4934370 (2015).
12. Gerken L R H et al. Catalytic activity imperative for nanoparticle dose enhancement in photon and proton therapy, Nature Communications, 13:3248, (2022) DOI: 10.1038/s41467-022-30982-5
13. Rudek B, et al, Radio-enhancement by gold nanoparticles and their impact on water radiolysis for x-ray, proton and carbon-ion beams, Phys. Med. Biol., **64**, 175005, (2019) DOI: 10.1088/1361-6560/ab314c.

14. Mohseni M. *et al*. Study on the dose enhancement of gold nanoparticles when exposed to clinical electron, proton, and alpha particle beams by means of Geant4. J. Med. Signals Sens. 2020; 10, 286–294. DOI: 10.4103/jmss.JMSS_58_19.
15. Cho J et al. Quantitative investigation of physical factors contributing to gold nanoparticle-mediated proton dose enhancement, Phys. Med. Biol. **61**, 2562-2581 (2016) DOI: 10.1088/0031-9155/61/6/2562.
16. McKinnon S. *et al*. Local dose enhancement of proton therapy by ceramic oxide nanoparticles investigated with Geant4 simulations. *Phys. Med.* **32**, 1584–1593; DOI: 10.1016/j.ejmp.2016.11.112 (2016).
17. Ahn S. H. Monte Carlo investigation of dose enhancement due to gold nanoparticle in carbon-12, helium-4, and proton beam therapy. *Prog. Med. Physic.* 33, 114–120; DOI: 10.14316/pmp.2022.33.4.114 (2022).
18. Walzlein C., Scifoni E., Kramer M. and Durante M. heavy atom nanoparticles irradiated by protons. Phys. Med. Biol. 2014; 59 1441–1458. DOI: 1088/0031-9155/59/6/1441.
19. Francis, Z., Montarou, G., Incerti, S., Bernal, M., Zein, S.A. A simulation study of gold nanoparticles localisation effects on radiation enhancement at the mitochondrion scale. *Phys. Med.* **67**, 148–154; DOI: 10.1016/j.ejmp.2019.10.038 (2019).
20. Velten C. and Tom´e W. A. Reproducibility study of Monte Carlo simulations for nanoparticle dose enhancement and biological modeling of cell survival curves. *Biomed. Phys. Eng. Express*. **9**;045004; DOI: 10.1088/2057-1976/acd1f1 (2023).
21. Peukert D., Kempson I., Douglass M. and Bezak E. Gold nanoparticle enhanced proton therapy: A Monte Carlo simulation of the effects of proton energy, nanoparticle size, coating material, and coating thickness on dose and radiolysis yield. Med. Phys; 47 (2), (2020)
22. Peukert D., Kempson I., Douglass M., and Bezak E. Gold Nanoparticle Enhanced Proton Therapy: Monte Carlo Modeling of Reactive Species' Distributions Around a Gold Nanoparticle and the Effects of Nanoparticle Proximity and Clustering, Int. J. Mol. Sci., 20:4280, (2019) DOI:10.3390/ijms20174280.
23. Rajabpour S., Saberi H., Rasouli J., and Jabbari N. Comparing Geant4 physics models for proton-induced dose deposition and radiolysis enhancement from a gold nanoparticle. *Scientific Reports*. **12**:1779; DOI: 10.1038/s41598-022-05748-0 (2022).
24. Huynh N. H. and Chow J. C. L. DNA dosimetry with Gold Nanoparticle Irradiated by Proton Beam: A Monte Carlo Study on Dose Enhancement. *Appl. Sci.* **11**, 10856; DOI: 10.3390/app112210856 (2021).
25. Jackson N., Cecchi D., Beckham W. and Chithrani D. B. Application of High-Z Nanoparticles to Enhance Current Radiotherapy Treatment, Molecules 2024; 29(11); 2438; DOI: .3390/molecules29112438.
26. Smith C. L. *et al*. Determination of dose enhancement caused by gold-nanoparticles irradiated with proton, X-rays (kV and MV) and electron beams, using alanine/EPR dosimeters. Radiation Measurements, 2015, 82, 122-128, DOI: 10.1016/j.radmeas.2015.09.008.
27. Liu Y, et al. The dependence of radiation enhancement effect on the concentration of gold nanoparticles exposed to low- and high-LET radiation, Physica Medica, Volume 31, Issue 3, 210-218, (2015) DOI: 10.1016/j.ejmp.2015.01.006. ?
28. Schlatholter T, et al. Improving proton therapy by metal-containing nanoparticles: nanoscale insights, International J of Nanomedicine, 1549-1556, (2016) DOI: 10.2147/IJN.S99410.
29. Li, S. *et al*. Antibody-functionalized gold nanoparticles as tumor targeting radiosensitizers for proton therapy. *Nanomedicine*, 14(3), 317-333, (2019) DOI: 10.2217/nnm-2018-0161.

30. Li, S. *et al*. LET-dependent radiosensitization effects of gold nanoparticles for proton irradiation, Nanotechnology, **27**, 455101 (2016) DOI: 10.1088/0957-4484/27/45/455101
31. Cunningham C, *et al*. Radiosensitization effect of gold nanoparticles in proton therapy, Front. Public Health, 9:699822 (2021) DOI: 10.3389/fpubh.2021.699822.
32. Hespeel F. *et al*. Experimental measurements validate the use of the binary encounter approximation model to accurately compute proton induced dose and radiolysis enhancement from gold nanoparticles. *Phys. Med. Biol.* **64**, 065014, DOI: 10.1088/1361-6560/ab0516 (2019).
33. Kim J. K. *et al*. Enhanced proton treatment in mouse tumors through proton irradiated nanoradiator effects on metallic nanoparticles. *Phys. Med. Biol.* **57**, 8309-8323; DOI: 10.1088/0031-9155/57/24/8309 (2012).
34. Penninckx S., Heuskin A. C., Michiels C., and Lucas S. Gold Nanoparticles as a Potent Radiosensitizer: A Transdisciplinary Approach from Physics to Patient. *Cancers*. **12**; DOI: 10.3390/cancers12082021 (2020).
35. Polf J. C. *et al*. Enhanced relative biological effectiveness of proton radiotherapy in tumor cells with internalized gold nanoparticles. *Appl. Phys. Lett*. **98**, 193702; DOI: 10.1063/1.3589914 (2011).
36. Chang-Yun Lo, et al, Gold-Nanoparticles-Enhanced Production of Reactive Oxygen Species in Cells at Spread-Out Bragg Peak under Proton Beam Radiation, ACS Omega, 8, 17922-17931 (2023) DOI: 10.1021/acsomega.3c01025.
37. Brero, F et al. Proton Therapy, Magnetic Nanoparticles and Hyperthermia as Combined Treatment for Pancreatic BxPC3 Tumor Cells. Nanomaterials, 13, 791, (2023) DOI: 10.3390/nano13050791
38. Cunningham C. et ai. Radiosensitization Effect of Gold Nanoparticles in Proton Therapy, Front. Public Health, 9:699822 (2021) DOI: 10.3389/fpubh.2021.699822.
39. Jeynes J. C. G. et al. Investigation of gold nanoparticle radiosensitization mechanisms using a free radical scavenger and protons of different energies, Phys. Med. Biol. 59, 6431-6443, (2014) DOI: 10.1088/0031-9155/59/21/6431.
40. Agostinelli S. et al. GEANT4-a simulation toolkit. Nucl. Instr. Methods: Sect. A. 506(**3**) 250–303; (2003).
41. Allison J. et al. GEANT4 development and applications. IEEE Transactions on Nuclear Science, Vol. 53, Issue 1, 270–278; (2006).
42. Tabbakh F. Significance of the Proton Energy Loss Mechanism to Gold Nanoparticles in Proton Therapy; A Geant4 Simulation. *Scientific Reports*, **14**:24978, (2024) DOI: 10.1038/s41598-024-76244-w.
43. Tabbakh F. Dose comparison of slowing-down protons and secondary electrons by gold nanoparticle in proton therapy: simulation study, Eur. Phys. J. Plus, 140:265, (2025) DOI: 10.1140/epjp/s13360-025-06197-0.
44. Berthel E, Ferlazzo M L, Devic C , Bourguignon M and Foray N. What Does the History of Research on the Repair of DNA Double-Strand Breaks Tell Us?—A Comprehensive Review of Human Radiosensitivity, Int. J of Mol. Sci. 20, 5339, (2019) DOI: 10.3390/ijms20215339.
45. Zhou H, Hong M, Chai Y, Hei TK. Consequences of cytoplasmic irradiation: studies from microbeam. J Radiat Res. 2009 Mar;50 Suppl A(0 0):A59-65. DOI: 10.1269/jrr.08120s. PMID: 19346686; PMCID: PMC3664637.
46. Mladenov E and Iliakis G (2011) The Pathways of Double-Strand Break Repair. DNA Repair - On the Pathways to Fixing DNA Damage and Errors. InTech. Available at: http://dx.doi.org/10.5772/24572.
47. Baatout S. (), Radiobiology textbook, Belgian Nuclear Research Centre (SCK CEN), ISBN 978-3-031-18810-7, DOI: 10.1007/978-3-031-18810-7.
48. Bobrowski K. (2012), Radiation-Induced Radical Reactions, Encyclopedia of Radicals in Chemistry, Biology and Materials, John Wiley, DOI: 10.1002/9780470971253.rad005

49. Gissela B, Ortiz-Lopez Rocio, Rojas-Martinez A (2015). Ionizing radiation-induced DNA injury and damage detection in patient with breast cancer, Genetic and Molecular Biology, 38, 4, 420-432. DOI: 10.1590/S1415-475738420150019.
50. Carbone G. G. *et al*. Exploring the potential of gold nanoparticles in proton therapy: mechanisms, advances, and clinical horizons, *Pharmeceutics*, 17, 176, (2025) DOI: 10.3390/pharmaceutics17020176.
51. Kwon J et al. Investigation of energy absorption by clustered gold nanoparticles, *Nuclear Inst. and Methods in Physics Research B*, 429, 34-41 (2018) DOI: 10.1016/j.nimb.2018.05.033.
52. Peckys D B and Jong N, Visualizing Gold Nanoparticle Uptake in Live Cells with Liquid Scanning Transmission Electron Microscopy, Nano Lett., 11, 1733-1738, (2011) DOI: 10.1021/nl200285r.
53. Hainfeld J F, Slatkin D N and Smilowitz H M. The use of gold nanoparticles to enhance radiotherapy in mice, *Phys. Med. Biol*. **49**, 309-315, (2004), DOI: 10.1088/0031-9155/49/18/N03.
54. Enferadi M *et al*.Radiosensitization of ultrasmall GNP-PEG-cRGDfK in ALTS1C1 exposed to therapeutic protons and kilovoltage and megavoltage photons, *International Journal of Radiation Biology*, (2017) DOI:10.1080/09553002.2018.1407462
55. Abdul Rashid R *et al*. Cell survival analysis of radiosensitization effects by gold nanoparticles for proton beam therapy, J of Radiation Research and Applied Sciences, 18, 101203, (2025) DOI: 10.1016/j.jrras.2024.101203.
56. Wang W et al, Modelling of Cellular Survival Following Radiation-Induced DNA Double-Strand Breaks, Scientific Reports, 8:16202, (2018) DOI: 10.1038/s41598-018-34159-3.
57. Ostashevsky J Y, Prediction of cell survival curves from DNA double-strand break repair data for low- and high-LET radiation.
58. Usami N et al. Fast He2+ ion irradiation of DNA loaded with platinum-containing molecules, *Int. J Radiat. Biol.*, Vol. 81, No. 7, 515-522, (2005) DOI: 10.1080/09553000500304318.
59. Porcel E, et al. Platinum nanoparticles: a promising material for future cancer therapy, Nanotechnology, 21, 085103, (2010), DOI: 10.1088/0957-4484/21/8/085103.
60. Jeynes J C G, Merchant M J, spindler A, Wera A-C, Kirkby K J, Investigation of gold nanoparticles radiosensitization mechanism using a free radical scavenger and protons of different energies, *Phys. Med. Biol*., 59, 6431-6443, (2014), DOI: 10.1088/0031-9155/59/21/6431.
61. Folkard M. *et al*. Inactivation of V79 cells by low-energy protons, deuterons and helium-3 ions, Int. J. Radiat. Biol. Vol. 69, NO. 6, 729-738, (1996).
62. Xu Long, Kainan Chong, Yutai Su, Leiming Du and Guoqi Zhang, Connecting the macroscopic and mesoscopic properties of sintered silver nanoparticles by crystal plasticity finite element method, *Engineering Fracture Mechanics*, Volume 281, 109137, (2023) DOI: 10.1016/j.engfracmech.2023.109137.
63. Yunbo Nie et al. Metal organic framework coated MnO2 nanosheets delivering doxorubicin and self-activated DNAzyme for chemo-gene combinatorial treatment of cancer, *International Journal of Pharmaceutics*, Volume 585, 119513, (2020) DOI: 10.1016/j.ijpharm.2020.119513.
64. Lulu Li, Yanmei Si, Binsheng He and Jishan Li, Au-Ag alloy/porous-SiO2 core/shell nanoparticle-based surface-enhanced Raman scattering nanoprobe for ratiometric imaging analysis of nitric oxide in living cells, Talanta, Volume 205, 120116, (2019) DOI: 10.1016/j.talanta.2019.120116.

Authors' contributions:

F.T. is the sole author and is responsible for conceptualization, methodology, software, validation, formal analysis, investigation, resources, data curation, writing the original draft, review & editing,

The conflict of interest statement: The author (s) of the present work declare no competing financial interests.

Funding: No funding was received for conducting this study.

Data availability: The datasets generated and/or analyzed during the current study are available from the corresponding author.

Ethics approval: In the present study no human (or animal) tissue was involved.